Developmental Biology 342 (2010) 96–107

Contents lists available at ScienceDirect

Developmental Biology

journal homepage: www.elsevier.com/developmentalbiology

MSP hormonal control of the oocyte MAP kinase cascade and reactive oxygen species signaling

Youfeng Yang [1], Sung Min Han, Michael A. Miller *

Department of Cell Biology, University of Alabama at Birmingham, Birmingham, AL 35294, USA

ARTICLE INFO

Article history:
Received for publication 27 October 2009
Revised 12 March 2010
Accepted 31 March 2010
Available online 7 April 2010

Keywords:
MSP
MAP kinase
Oocyte maturation
Shp
RasGAP
Ras
Fertilization
SOD1
Amyotrophic lateral sclerosis
VAPB
Reactive oxygen species

ABSTRACT

The MSP domain is a conserved immunoglobulin-like structure that is important for *C. elegans* reproduction and human motor neuron survival. *C. elegans* MSPs are the most abundant proteins in sperm, where they function as intracellular cytoskeletal proteins and secreted hormones. Secreted MSPs bind to multiple receptors on oocyte and ovarian sheath cell surfaces to induce oocyte maturation and sheath contraction. MSP binding stimulates oocyte MPK-1 ERK MAP Kinase (MAPK) phosphorylation, but the function and mechanism are not well understood. Here we show that the Shp class protein-tyrosine phosphatase PTP-2 acts in oocytes downstream of sheath/oocyte gap junctions to promote MSP-induced MPK-1 phosphorylation. PTP-2 functions in the oocyte cytoplasm, not at the cell surface to inhibit multiple RasGAPs, resulting in sustained Ras activation. We also provide evidence that MSP promotes production of reactive oxygen species (ROS), which act as second messengers to augment MPK-1 phosphorylation. The Cu/Zn superoxide dismutase SOD-1, an enzyme that catalyzes ROS breakdown in the cytoplasm, inhibits MPK-1 phosphorylation downstream of or in parallel to *ptp-2*. Our results support the model that MSP triggers PTP-2/Ras activation and ROS production to stimulate MPK-1 activity essential for oocyte maturation. We propose that secreted MSP domains and Cu/Zn superoxide dismutases function antagonistically to control ROS and MAPK signaling.

Published by Elsevier Inc.

Introduction

The major sperm protein (MSP) domain folds into an approximately 120 amino acid immunoglobulin-like seven-stranded beta sandwich that is conserved throughout eukaryotic evolution (Bullock et al., 1996; Han et al., 2009). This domain was initially identified in *C. elegans* MSPs, the most abundant proteins in sperm (Klass and Hirsh, 1981). MSPs function as secreted hormones (Kosinski et al., 2005; Miller et al., 2001) and intracellular cytoskeletal proteins (Bottino et al., 2002). The ancestral MSP domain-containing proteins are VAPs (VAMP/synaptobrevin-associated proteins), which contain an N-terminal MSP domain, a coiled coil motif, and a transmembrane-spanning region (Han et al., 2009). A P56S substitution in the human VAPB MSP domain is associated with a dominantly inherited form of amyotrophic lateral sclerosis (ALS), an adult onset motor neuron degenerative disorder (Nishimura et al., 2004). We have recently shown that MSPs and VAP MSP domains have an evolutionarily conserved signaling function and that the P56S mutation prevents MSP domain secretion (Tsuda et al., 2008). The most extensively characterized gene associated with ALS is *sod1*, a cytosolic Cu/Zn superoxide dismutase (Rosen et al., 1993). However, the mechanisms by which *sod1* and *vapb* mutations influence ALS pathogenesis are not clear.

C. elegans oocytes become fertilizable through a process called oocyte maturation, characterized by the transition from meiotic prophase to metaphase I, cytoskeletal rearrangement, and meiotic spindle assembly (Greenstein, 2005). Sperm secrete MSP to induce oocyte maturation and ovarian sheath contraction, which together facilitate fertilization (Kosinski et al., 2005; Miller et al., 2001) (Fig. 1A). MSP signal transduction involves incompletely understood hierarchies in oocytes and sheath cells (Han et al., 2009). MSP binds to multiple receptors on oocyte and sheath surfaces, including the VAB-1 Eph receptor protein-tyrosine kinase (Govindan et al., 2006; Miller et al., 2003). These receptor pathways influence oocyte maturation, as well as other processes such as oocyte growth, microtubule reorganization, and large ribonucleoprotein foci disassembly (Harris et al., 2006; Jud et al., 2008; Nadarajan et al., 2009). $G_{\alpha s}$-adenylate cyclase signaling is required in sheath cells to induce oocyte maturation, suggesting that sheath cells are critical MSP sensors (Govindan et al., 2006; Govindan et al., 2009) (Fig. 1A). MSP binding antagonizes gap junctional communication between oocytes and sheath cells (Govindan et al., 2006; Whitten and Miller, 2007). Downstream of sheath/oocyte gap junctions is oocyte MPK-1 ERK MAP Kinase (MAPK) (Church et al., 1995), which becomes phosphorylated throughout the cytosol (Miller et al., 2001). MPK-1

* Corresponding author. Tel.: +1 205 996 2096.
E-mail address: mamiller@uab.edu (M.A. Miller).
[1] Y. Y. conducted all experiments except the oxygen consumption assays.

0012-1606/$ – see front matter. Published by Elsevier Inc.
doi:10.1016/j.ydbio.2010.03.026

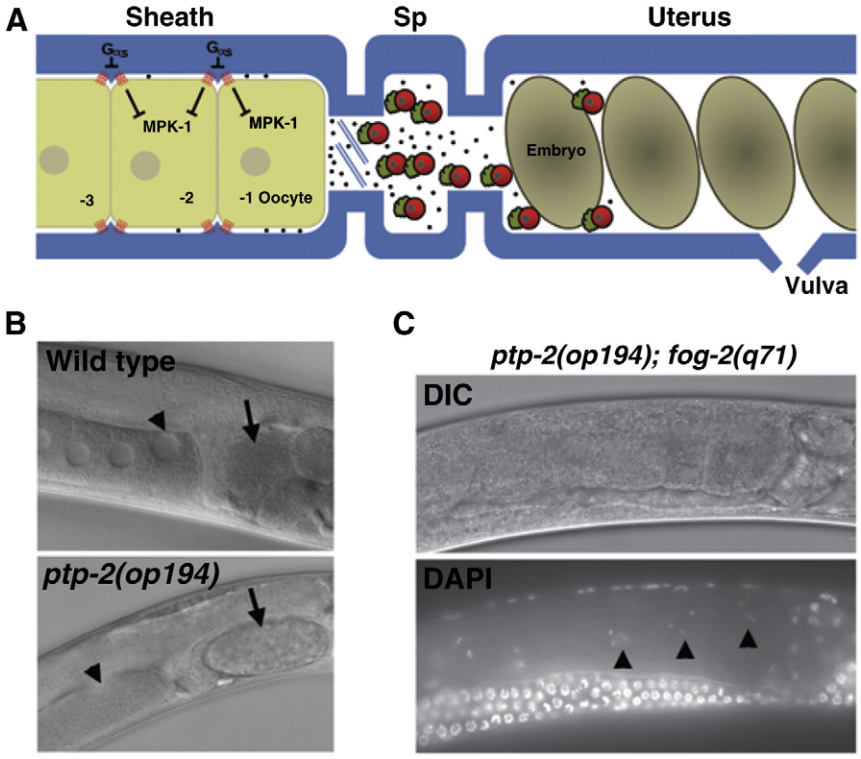

Fig. 1. The *C. elegans* proximal gonad and *ptp-2* mutant phenotype. (A) Diagram of the wild-type hermaphrodite proximal gonad. The oocyte closest to the spermatheca (Sp) is called the −1 oocyte. Sperm (red) secrete the protein hormone MSP (black dots) to induce MPK-1 phosphorylation, oocyte maturation, and sheath cell contraction, which together facilitate ovulation. In *fog-2*(*q71*) and *fog-3*(*q443*) mutant females, all germ cells develop into oocytes, which arrest in diakinesis of meiotic prophase in the absence of male sperm. Oocytes mature sequentially every 20–25 min in the presence of sperm/MSP. (B) DIC micrograph of wild-type and *ptp-2*(*op194*) mutant gonads. The arrowhead points to the oocyte adjacent to the spermatheca (-1 oocyte). The arrow points to a fertilized embryo. Notice that the single fertilized embryo in the *ptp-2* mutant uterus is large and has completed multiple cell divisions, contrasting with the smaller wild-type embryo that has not yet divided. (C) DIC and DAPI micrographs of an unmated *ptp-2*(*op194*); *fog-2*(*q71*) female. The arrowheads indicate diakinesis stage oocytes.

phosphorylation occurs late in the MSP signaling response, just prior to nuclear envelope breakdown (Han et al., 2009).

The MAPK cascade, including KSR-2 Kinase Suppressor of Ras, LET-60 Ras, LIN-45 Raf, MEK-2 MAP kinase kinase, and MPK-1 MAPK has an essential function in promoting progression through meiotic pachytene (Church et al., 1995; Hsu et al., 2002; Ohmachi et al., 2002). MPK-1 is expressed throughout the germ line, where it is primarily regulated by phosphorylation (Lee et al., 2007). Analyses of loss of function and gain of function alleles support roles for the MAPK cascade in regulating oocyte pachytene progression, growth, differentiation, and possibly oocyte maturation. A major hindrance to studying the MAPK cascade in MSP signaling is the earlier roles. For example, loss of function mutations in *let-60*, *lin-45*, and *mpk-1* prevent progression to diakinesis and oocyte development. Questions such as what is the role of the MAPK cascade during oocyte maturation and how is this cascade regulated have been difficult to address. The PTP-2 SH2 domain-containing tyrosine phosphatase has been identified as an upstream regulator of Ras during oogenesis (Gutch et al., 1998). PTP-2 is homologous to *Drosophila* Corkscrew (CSW) and mammalian Shp1 and Shp2. These phosphatases comprise a highly conserved subfamily thought to promote sustained MAPK signaling downstream of receptor activation (Feng, 1999; Neel et al., 2003). A null mutation in *ptp-2* causes abnormally large oocytes and low brood size (Gutch et al., 1998). We have shown that *ptp-2* mutant hermaphrodites have low oocyte maturation rates and MPK-1 phosphorylation levels (Miller et al., 2004). Whether or not these defects are due to impaired MSP signaling or abnormal oogenesis is not clear. Based on these studies, PTP-2 might provide a key entry point for understanding MPK-1 functions and regulation during MSP signaling.

Here, we show that MSP induces PTP-2/Ras activation and reactive oxygen species (ROS) signaling to promote MPK-1 activation. We show that *ptp-2* mutant oocytes progress to diakinesis, disassemble the nucleoleus, and initiate chromosome condensation, but fail to phosphorylate MPK-1 and complete maturation in response to MSP. Our results support the model that PTP-2 acts in oocytes downstream of sheath/oocyte gap junctions to antagonize RasGAP activity and promote sustained Ras activation essential for oocyte maturation. In a second mechanism, MSP stimulates ROS production to augment MPK-1 phosphorylation. The Cu/Zn superoxide dismutase SOD-1 inhibits this mechanism downstream of or in parallel to *ptp-2*. We propose that Cu/Zn superoxide dismutases breakdown cytosolic ROS important for MSP domain signal transduction.

Results

ptp-2 functions in sperm-dependent oocyte maturation, but not sheath contraction

To investigate the mechanism(s) by which MSP regulates MPK-1 activity, we decided to characterize the Shp class phosphatase PTP-2. Previous studies have shown that *ptp-2(op194)* mutants have oocyte maturation and MPK-1 phosphorylation defects, but it is not clear whether these defects are due to abnormal oogenesis or meiotic progression. The *op194* allele deletes the phosphatase domain and is a null allele (Gutch et al., 1998). First, we monitored oocyte development and oocyte maturation by DIC microscopy. The *ptp-2(op194)* mutant strains used in our studies contain the linked *unc-4(e120)* allele for genotype scoring (Miller et al., 1992). *unc-4* encodes a paired-class homeodomain protein expressed in motor

Table 1
Oocyte maturation rates.

Genotype	Sperm (Y/N)	Maturations per hour	N
1. Wild type	Y	2.58 ± 0.33	15
2. *unc-4(e120)*	Y	2.53 ± 0.45	13
3. *ptp-2(op194)* L4 + 36 h	Y	0.10 ± 0.11	14
4. *ptp-2(op194)* L4+16 h	Y	0.63 ± 0.24	14
5. *fog-2(q71)*	N	0.08 ± 0.09	10
6. *fog-2(q71)* x *fog-2(q71)* male	Y	2.45 ± 0.28	9
7. *ptp-2(op194); fog-2(q71)* L4 + 36 h x *fog-2(q71)* male	Y	0.07 ± 0.09	8
8. *ptp-2(op194); fog-2(q71)* L4+16 h x *fog-2(q71)* male	Y	0.36 ± 0.32	8
9. *fog-2(q71)* + Buffer alone	N	0.05 ± 0.11	10
10. *fog-2(q71)* + 200nM MSP	N	1.13 ± 0.40	10
11. *ptp-2(op194); fog-2(q71)* + 200nM MSP	N	0.03 ± 0.08	10
12. *let-60(n1046gf)*	Y	2.34 ± 0.94	15
13. *ptp-2(op194); let-60(n1046gf)*	Y	2.20 ± 0.97	15
14. *let-60(n1046); fog-3(q443)*	N	0.20 ± 0.20	12
15. *ptp-2(op194); gap-1(ga133)*	Y	0.29 ± 0.24	10
16. *ptp-2(op194); gap-2(tm748)*	Y	0.02 ± 0.04	10
17. *ptp-2(op194); gap-1(ga133); gap-2(tm748)*	Y	1.30 ± 0.36	10
18. *ptp-2(op194) inx-14* RNAi	Y	0.11 ± 0.13	9
19. *ptp-2(op194) inx-22* RNAi	Y	0.13 ± 0.19	8
20. *fog-2(q71) inx-14* RNAi	N	0.66 ± 0.35	8
21. *fog-2(q71) inx-22* RNAi	N	0.75 ± 0.44	8
22. *ptp-2(op194); unc-43(n498gf)*	Y	0.19 ± 0.10	16
23. *sod-1(tm776)*	Y	2.74 ± 0.23	15
24. *sod-1(tm776); fog-2(q71)*	N	0.13 ± 0.14	10

See text for details. Average value ± standard deviation is shown. All *ptp-2(op194)* strains contain the *unc-4(e120)* allele. The oocyte maturation rate of unmated *fog-3(q443)* females is not significantly different than unmated *fog-2(q71)* females (Corrigan et al., 2005). The *fog-2(q71)* allele does not affect male reproductive capacity or sperm function.

neurons and the *e120* allele does not influence oocyte maturation (Table 1, compare lines 1 and 2; $P>0.05$). As previously reported (Gutch et al., 1998), proximal gonads of *ptp-2(op194)* mutants contain developing oocytes, with the most proximal oocyte (−1 position) often significantly larger than the others and wild-type oocytes (Fig. 1A and B). *ptp-2* mutant gonads contain fewer oocytes than wild-type gonads, consistent with delayed pachytene progression and oocyte development. Oocyte maturation was directly observed in two cases. Both times it occurred normally and was followed by successful ovulation and fertilization. *ptp-2* mutant hermaphrodites typically contain 1–5 fertilized eggs undergoing embryonic development in the uterus, but not unfertilized eggs (Fig. 1B). These observations support the idea that *ptp-2* mutant oocytes are competent to undergo oocyte maturation. Proximal gonads of older mutant hermaphrodites sometimes contain degenerating or abnormally developing oocytes.

The oocyte maturation rate of adult *ptp-2(op194)* mutants is low, much less than the rate of wild-type and *unc-4(e120)* controls (Table 1, compare line 3 to lines 1 and 2; $P<0.001$). The maturation rate of young adult mutants (16–20 h post L4) is higher than adult mutants (36–40 h post L4), due either to maternally derived *ptp-2* or a *ptp-2*-independent mechanism (Table 1, compare lines 3 and 4). The low oocyte maturation rate of *ptp-2* mutants is not rescued by mating to wild-type males, even though abundant male-derived sperm accumulate in the spermatheca (data not shown). We constructed *ptp-2(op194); fog-2(q71)* double mutant females and measured oocyte maturation rates in the presence and absence of sperm. Unmated *ptp-2(op194); fog-2(q71)* females accumulate diakinesis-stage oocytes in the proximal gonad, as judged using the DNA stain 4', 6-diamidino-2-phenylindole (DAPI) (Fig. 1C). Mating the *ptp-2* mutant females to *fog-2(q71)* males, which have fully functional sperm (Schedl and Kimble, 1988) (Table 1, lines 5 and 6), does not promote an oocyte maturation rate increase in adults, but does promote a small increase in young females (Table 1, compare lines 5–8). We conclude that the *ptp-2* mutant oocyte maturation defect is not due to defective sperm.

MSP stimulates an increase in the basal sheath contraction rate. *ptp-2* is not required for this response, as *ptp-2(op194)* hermaphrodites and mated *ptp-2(op194); fog-2(q71)* females have higher basal contraction rates than unmated female controls (Table 2, compare lines 1–4; $P<0.001$). In addition to sheath contraction, MSP promotes sustained actomyosin-dependent cytoplasmic streaming that drives oocyte growth (Govindan et al., 2009; Nadarajan et al., 2009). The oocytes of unmated *ptp-2(op194); fog-2(q71)* females are smaller than those of *ptp-2(op194)* hermaphrodites (Fig. 1B and C) and resemble oocytes from unmated female controls. These results demonstrate that *ptp-2* is not required for basal sheath contraction and oocyte growth. Collectively, the data support the hypothesis that *ptp-2* mutants receive MSP signals, but fail to respond with an oocyte maturation rate increase.

ptp-2 mutant oocytes fail to fully activate MPK-1 and exit meiotic prophase rapidly

We used molecular markers to evaluate the developmental status of *ptp-2* mutant oocytes. The monoclonal antibody MAPK-YT detects the diphosphorylated, activated form of MPK-1 (dpMPK-1) (Lee et al., 2007; Miller et al., 2001; Page et al., 2001). In wild-type gonads, dpMPK-1 is often seen throughout the cytoplasm and nucleus of the −1 to −3 oocytes, with highest levels in the −1 oocyte. In contrast, we rarely detect dpMPK-1 in oocytes of *ptp-2* mutant hermaphrodites or mated *ptp-2(op194); fog-2(q71)* females (Fig. 2 and data not shown). The low dpMPK-1 levels in *ptp-2* mutant hermaphrodite gonads resemble unmated female gonads (Fig. 2). Therefore, *ptp-2* is required for elevated MPK-1 activity in the most proximal oocytes.

DAPI was used to evaluate oocyte meiotic progression. DAPI staining of *ptp-2(op194)* gonads shows the oocytes progress to diakinesis of meiotic prophase, similar to wild-type and unmated females (Fig. 2). Another marker for developmental status is the nucleolus, which is present in developing oocytes transitioning through meiotic prophase (McCarter et al., 1999). The nucleolus disappears about 70 min before nuclear envelope breakdown. Nucleolar disappearance is not sperm-dependent, as it occurs in unmated *fog-2(q71)* females. DIC microscopy and an antibody against the nucleolar marker Nop1 (Aris and Blobel, 1989; Burrows et al., 2006; Henriquez et al., 1990) indicate that the nucleolus disappears in *ptp-2* mutant oocytes (Fig. 2). Nop1 distribution in *ptp-2(op194)* mutant gonads resembles that of unmated females. These data support the hypothesis that *ptp-2* mutant oocytes are competent to undergo oocyte maturation.

M-phase entry can be monitored in maturing oocytes using an antibody specific for phosphorylated histone H3 at serine 10 (pH3), a marker for chromosome condensation (Hsu et al., 2000). In wild-type gonads, anti-pH3 antibodies stain chromosomes of the −1 to −3 oocytes in a sperm-dependent manner. We often detected *ptp-2* mutant oocytes whose chromosomes stained with anti-pH3 antibodies (Fig. 2), suggesting that *ptp-2(op194)* mutant oocytes initiate M-phase entry,

Table 2
Ovarian sheath cell contraction rates.

Genotype	Sperm (Y/N)	Contractions per minute	N
1. Wild type	Y	9.63 ± 1.17	10
2. *ptp-2(op194)*	Y	9.83 ± 1.91	12
3. *ptp-2(op194); fog-2(q71)*	N	1.50 ± 1.00	12
4. *ptp-2(op194); fog-2(q71)* x *fog-2(q71)* male	Y	8.79 ± 1.61	11
5. *fog-2(q71)* + Buffer alone	N	2.03 ± 0.81	11
6. *fog-2(q71)* + 200nM MSP	N	7.30 ± 2.08	10
7. *ptp-2(op194); fog-2(q71)* + 200nM MSP	N	7.94 ± 2.13	14

See text for details. Average value ± standard deviation is shown. All *ptp-2(op194)* strains contain the *unc-4(e120)* allele, which does not influence sheath contraction. *fog-2(q71)* females are unmated unless stated otherwise.

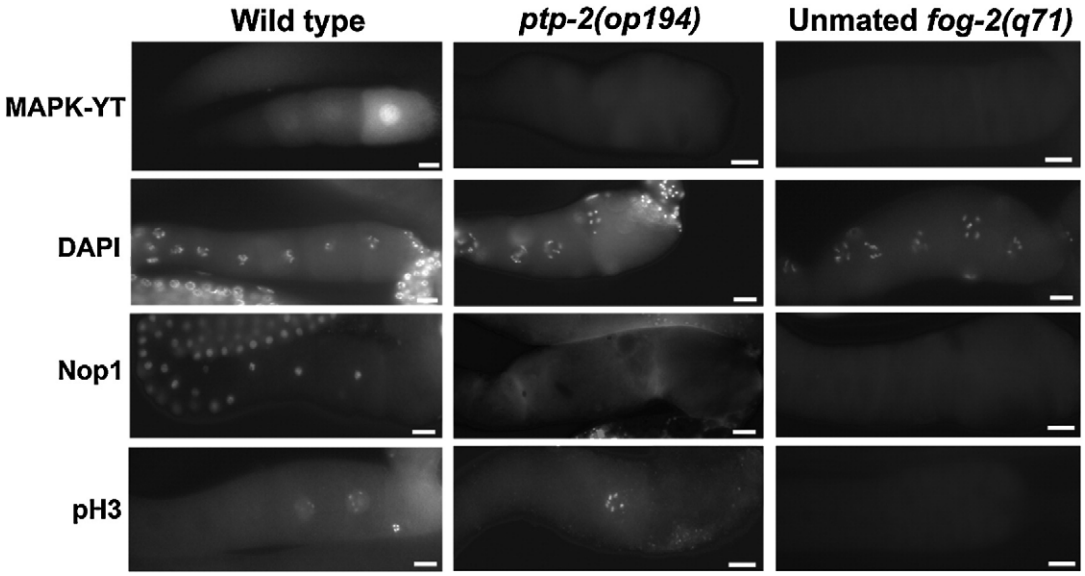

Fig. 2. Molecular characterization of wild-type hermaphrodite, *ptp-2* mutant hermaphrodite, and unmated female proximal gonads. The proximal gonad is in the same orientation as Fig. 1A, with the spermatheca to the right. The MAPK-YT, anti-Nop1, and anti-pH3 antibodies are described in the text. Scale bars, 20 μm.

but are slow to undergo nuclear envelope breakdown and progress to metaphase.

Our data indicate that *ptp-2* is required for the sperm-dependent increase in the oocyte maturation rate. Purified recombinant MSP directly microinjected into the reproductive tract of unmated females stimulates oocyte maturation and basal sheath contraction (Miller et al., 2001; Tsuda et al., 2008). MSP diffuses into the proximal gonad, where it binds to cell surface receptors (Miller et al., 2003). To test whether *ptp-2* is necessary for MSP-induced oocyte maturation, we microinjected 200 nM recombinant MSP into unmated *ptp-2(op194)* and control females. MSP does not stimulate the oocyte maturation rate of unmated *ptp-2(op194); fog-2(q71)* females (Table 1, compare lines 9–11; $P>0.05$). In contrast, MSP does stimulate an increase in the basal sheath contraction rate of unmated *ptp-2(op194); fog-2(q71)* females and control *fog-2(q71)* females (Table 2, compare lines 6 and 7 to line 5; $P<0.001$). MSP-induced sheath contraction is observed in the same *ptp-2* mutant gonads that fail to undergo oocyte maturation. We considered the possibility that *ptp-2* is required for surface expression of MSP receptors. To examine MSP receptor expression, we incubated dissected gonads with 200nM recombinant 6His-MSP conjugated to fluorescein (MSP-FITC). MSP-FITC binding is specific and requires cell surface receptor expression (Miller et al., 2003; Tsuda et al., 2008). In wild-type and *ptp-2(op194)* gonads, MSP-FITC binds extensively to the oocyte and sheath interface (Fig. S1). Taken together, these results support the model that *ptp-2* acts downstream of MSP to promote sustained MPK-1 activity essential for high oocyte maturation rates.

ptp-2 acts upstream of Ras and multiple RasGAPs

The brood size defect of *ptp-2(op194)* mutants is suppressed by the *let-60(n1046)* and *let-60(n1700)* gain of function alleles (Gutch et al., 1998). To examine oocyte maturation, we generated *ptp-2 (op194); let-60(n1046)* double mutants. Observation by DIC microscopy indicates that *ptp-2(op194)* oocyte maturation and oocyte growth defects are suppressed by the *n1046* gain of function allele. The *ptp-2(op194); let-60(n1046gf)* oocyte maturation rate is much higher than the *ptp-2(op194)* mutant rate (Table 1, compare line 13 to 3; $P<0.001$) and is similar to the *let-60(n1046gf)* and wild-type rates (Table 1, lines 1, 12, and 13). Next, we examined MPK-1 phosphorylation using the MAPK-YT antibody. *ptp-2(op194); let-60 (n1046gf)* mutants have more dpMPK-1 than *ptp-2(op194)* mutants, but less than wild-type and *let-60(n1046gf)* mutants (Fig. 3A–D). These data support the hypothesis that *ptp-2* functions upstream of or in parallel to *let-60* Ras to stimulate MPK-1 activation and oocyte maturation.

To test whether Ras activation is sufficient to promote oocyte maturation in the absence of MSP, we generated *let-60(n1046gf); fog-3(q443)* females. The oocyte maturation rate of unmated *let-60 (n1046gf); fog-3(q443)* females is similar to the rate of unmated control females (Table 1, compare lines 14 and 5). Furthermore, we did not detect elevated dpMPK-1 levels in the most proximal oocytes (Fig. 3E). Mating unmated *let-60(n1046gf); fog-3(443)* females to wild-type males stimulates the oocyte maturation rate and induces MPK-1 phosphorylation (data not shown). Similar results were observed in mated and unmated *ptp-2(op194); let-60(n1046gf); fog-3(443)* females. Therefore, increased Ras activity is not sufficient to induce MPK-1 phosphorylation and oocyte maturation in the absence of MSP.

In *Drosophila* embryos, CSW dephosphorylates a RasGAP binding site on the RTK Torso, preventing RasGAP recruitment (Cleghon et al., 1998). Of the three RasGAPs identified in *C. elegans* (Hajnal et al., 1997; Stetak et al., 2008), *gap-3* is implicated in oocyte pachytene progression. To avoid potential indirect interactions due to pachytene defects, we focused on *gap-1* and *gap-2* (Stetak et al., 2008). Double and triple mutant strains were constructed for oocyte maturation and MPK-1 activation analyses. The oocyte maturation rate of *gap-1(ga133); gap-2(tm748); ptp-2(op194)* mutants is significantly higher than the rates of *ptp-2(op194)* mutants, *gap-2 (tm748); ptp-2(op194)* mutants, and *gap-1(ga133); ptp-2(op194)* mutants (Table 1, compare line 17 to lines 3, 15, and 16; $P<0.001$). The triple mutant strain is viable, contrasting with *ptp-2(op194)* mutants. Therefore, loss of *gap-1* and *gap-2* together can partially suppress the oocyte maturation and viability defects of *ptp-2* mutants. The *gap-1(ga133); ptp-2(op194)* maturation rate is slightly higher than the *ptp-2(op194)* rate (Table 1, compare lines 15 and 3), indicating that loss of *gap-1* alone causes a mild suppressive effect. Oocyte dpMPK-1 levels in *gap-1(ga133); gap-2(tm748); ptp-2 (op194)* hermaphrodites are higher than *ptp-2(op194)* mutants, but less than the wild type (Fig. 3F). These results support the hypothesis that *ptp-2* functions upstream of multiple RasGAPs to promote Ras activation and oocyte maturation.

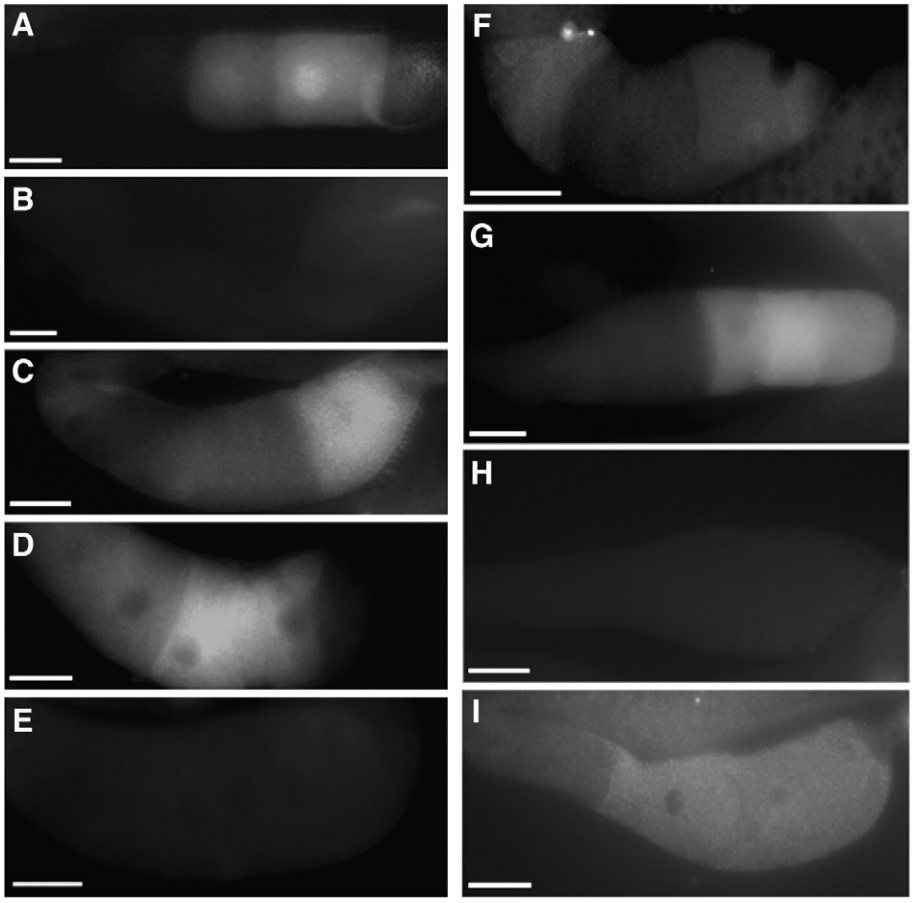

Fig. 3. MPK-1 MAPK activity in wild-type and mutant gonads. Dissected proximal gonads were incubated with MAPK-YT antibodies, which recognize the diphosphorylated form of MPK-1. Panels are (A) wild type, (B) *ptp-2*(*op194*), (C) *ptp-2*-(*op194*); *let-60*(*n1046gf*), (D) *let-60*(*n1046gf*), (E) unmated *let-60*(*n1046*); *fog-2*(*q71*) female, (F) *ptp-2*(*op194*); *gap-1* (*ga133*); *gap-2*(*tm748*), (G) *vab-1* RNAi, (H) *vab-1* RNAi *ptp-2*(*op194*), and (I) *ptp-2*(*op194*); *pie-1p::gfp::ptp-2*. Gonad orientation is with spermatheca to the right. Scale bars, 20 μm.

ptp-2 acts downstream of sheath/oocyte gap junctions

The MSP receptor *vab-1* negatively regulates MPK-1 phosphorylation in hermaphrodites. *vab-1* null mutant and RNAi hermaphrodite gonads have more oocytes containing phosphorylated MPK-1 than wild-type hermaphrodite gonads. To test the genetic relationship between *vab-1* and *ptp-2*, we examined MPK-1 phosphorylation in single and double knockouts. Contrasting with MPK-1 levels in *vab-1* RNAi gonads (Fig. 3G), MPK-1 phosphorylation levels in *vab-1* RNAi *ptp-2(op194)* gonads (Fig. 3H) resemble those in *ptp-2(op194)* gonads (Fig. 3B). These data support the idea that *ptp-2* acts downstream of *vab-1*. The *unc-43* CaMKII homolog (Reiner et al., 1999) is an MSP-responsive effector that functions in oocytes and sheath cells (Corrigan et al., 2005). An *unc-43(n498)* gain of function mutation causes elevated oocyte maturation and MPK-1 activation in the absence of MSP. To examine the genetic interaction between *unc-43* and *ptp-2*, we generated *ptp-2(op194); unc-43(n498gf)* double mutants. The oocyte maturation rate of the double mutants is similar to *ptp-2(op194)* single mutants (Table 1, compare line 22 to line 3). *unc-43(n498gf)* does suppress the *ptp-2(op194)* oocyte size defect, suggesting that the genetic hierarchies regulating oocyte growth and maturation are different. These results are consistent with the model that *ptp-2* acts downstream of *vab-1* and *unc-43* to regulate MPK-1 activity.

The $G_{\alpha s}$ heterotrimeric G protein subunit GSA-1 is required in sheath cells to promote MSP-induced oocyte maturation (Govindan et al., 2009). The oocyte maturation defect caused by sheath *gsa-1* loss is suppressed by loss of the innexins *inx-14* or *inx-22* (Govindan et al., 2006; Govindan et al., 2009). *inx-14* and *inx-22* are thought to form sheath/oocyte gap junctions that negatively regulate oocyte maturation in the absence of MSP (Govindan et al., 2006; Whitten and Miller, 2007). To examine the genetic relationship between *ptp-2* and gap junctions, we reduced *inx-14* and *inx-22* function by RNAi in *ptp-2 (op194)* mutants. *inx-14* or *inx-22* RNAi does not suppress the *ptp-2* mutant oocyte maturation and fertility defects (Table 1, compare lines 18 and 19 to line 3). In control females, *inx-14* and *inx-22* RNAi caused increased oocyte maturation rates (Table 1, compare lines 20 and 21 to line 5). Next, we tested the genetic relationship between *ptp*-2 and gap junctions in the absence of MSP. Unmated *inx-22(tm1661); fog-2 (q71)* females have high oocyte maturation rates (Whitten and Miller, 2007). To test whether this defect is dependent on *ptp-2*, we generated *inx-22(tm1661); ptp-2(op194); fog-2(q71)* triple mutants. In contrast to unmated *inx-22(tm1661); fog-2(q71)* females, the oocyte maturation rate of unmated triple mutant females is low and few oocytes accumulate in the uterus (Fig. 4A–C). Taken together, these results support the hypothesis that *ptp-2* functions downstream of sheath/oocyte gap junctions.

Germline PTP-2 expression partially rescues ptp-2 null oocyte maturation defects

The *ptp-2* gene lies within a large operon containing eight genes with internal promoters. A previous study showed that the ~600 base pairs upstream of the *ptp-2* translational start site were sufficient to drive GFP expression in a subset of head neurons, the intestine, spermatheca, and body wall muscle (Vazquez-Manrique et al., 2007). To test whether additional upstream sequences could influence expression, we generated transgenic lines containing

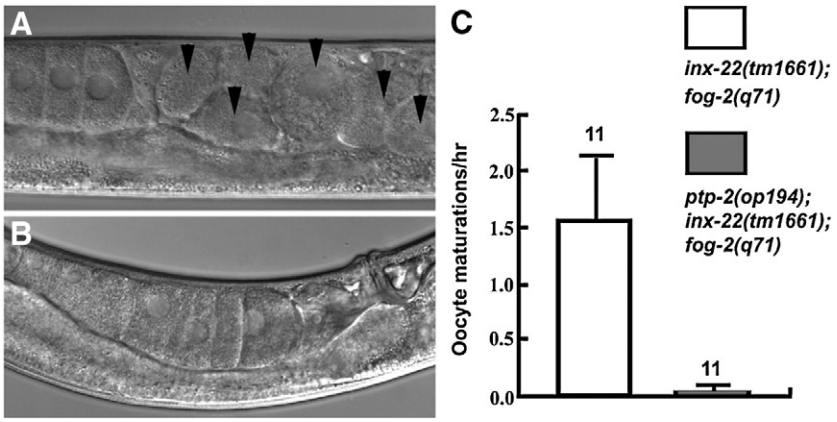

Fig. 4. Genetic relationship between *ptp-2* and the innexin *inx-22*. (A, B) DIC micrographs of (A) unmated *inx-22(tm1661); fog-2(q71)* females and (B) unmated *ptp-2(op194); inx-22 (tm1661); fog-2(q71)* females. Arrowheads indicate unfertilized oocytes in the uterus that have undergone oocyte maturation and ovulation. Gonad orientation is with spermatheca to the right. (C) Quantification of oocyte maturation rates. N is shown above error bars, which represent standard deviation.

genomic DNA ~5 kilobase pairs upstream of the *ptp-2* translational start site fused to the GFP coding sequence. These lines express GFP in head neurons, the intestine, and body wall muscle, similar to the smaller genomic construct. We also observed GFP in embryos, the developing vulva, and the adult gonadal sheath cells (Fig. 5).

ptp-2 mRNAs are abundantly expressed in the germ line (Reinke et al., 2004; Reinke et al., 2000). Our genetic data suggest that PTP-2 functions in oocytes downstream of sheath/oocyte gap junctions and upstream of *let-60* Ras. The microinjection method used to generate *ptp-2p::gfp* transgenic lines is not reliable for evaluating oocyte expression due to frequent silencing of the high copy arrays in the germ line (Praitis et al., 2001). To test whether PTP-2 expression in oocytes is sufficient to rescue the oocyte maturation defects, we generated transgenic lines by microparticle bombardment that express GFP::PTP-2 under control of the *pie-1* germline promoter (Tenenhaus et al., 1998; Tenenhaus et al., 2001). Microparticle bombardment generates low copy transgenic lines that sometimes escape the germ line silencing machinery (Praitis et al., 2001). Two independent lines show faint GFP expression throughout the cytoplasm of germ cells and oocytes, but not in the nuclei (Fig. 6A). Numerous other lines did not contain detectable GFP expression. To examine the subcellular localization in better detail, we dissected gonads out of the animal. GFP::PTP-2 was seen in the cytoplasm, sometimes associated with vesicle-like structures, but not at the cell surface (Fig. 6B). This pattern contrasts with the localization of MSP receptors, which are abundant at the oocyte cell surface (Fig. S1).

To determine whether germline GFP::PTP-2 could rescue the *ptp-2* mutant defects, we crossed the transgene into the *ptp-2(op194)* background. The genotype was confirmed by PCR. Germline expression of GFP::PTP-2 is sufficient to partially rescue the *ptp-2* null mutant oocyte maturation defect, embryonic lethality, and larval lethality (Fig. 6C). In addition, MPK-1 phosphorylation is detected in the most proximal oocytes (Fig. 3G). These data support to the hypothesis that PTP-2 functions in oocytes to regulate oocyte maturation and MPK-1 activation.

sod-1 negatively regulates MPK-1 phosphorylation

To identify additional mechanisms important for MPK-1 activity, we focused on ROS, which have been implicated in regulating MAPK in cultured cells (Abe et al., 2000; Aikawa et al., 1997; Secondo et al., 2008). The Cu/Zn superoxide dismutase SOD-1 converts ROS to oxygen or hydrogen peroxide. Dominant mutations in *sod1* and *vapb* are associated with ALS, but the genetic relationship between these genes, if any, is uncertain (Nishimura et al., 2004; Rosen et al., 1993). To test whether *C. elegans* SOD-1 regulates oocyte MPK-1 phosphorylation, we examined *sod-1(tm776)* null mutants (Yanase et al., 2009). Approximately twice as many oocytes contain dpMPK-1 in *sod-1* null gonads

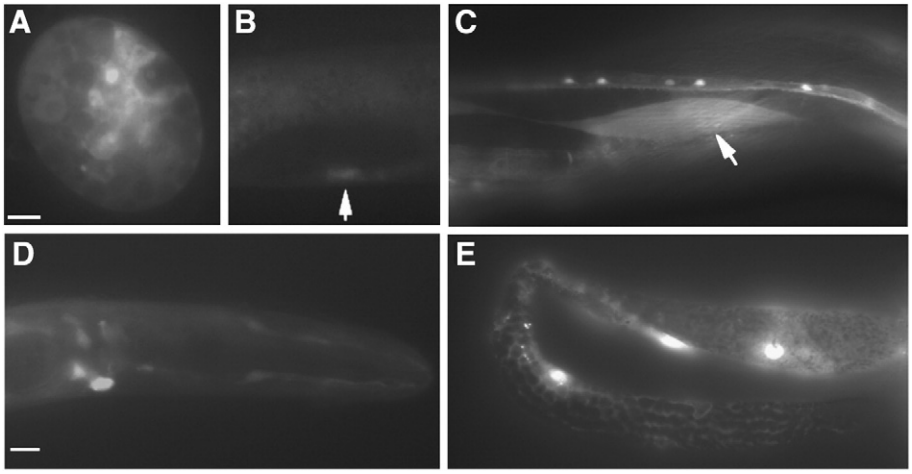

Fig. 5. *ptp-2* expression. (A–E) Genomic DNA (~5 kb) upstream of the *ptp-2* translational start site drives GFP expression in embryonic cells (A), the developing vulva (B, arrow), adult body wall muscle (C, arrow), adult head neurons (D), and adult gonadal sheath cells (E). Scale bars, 10 μm.

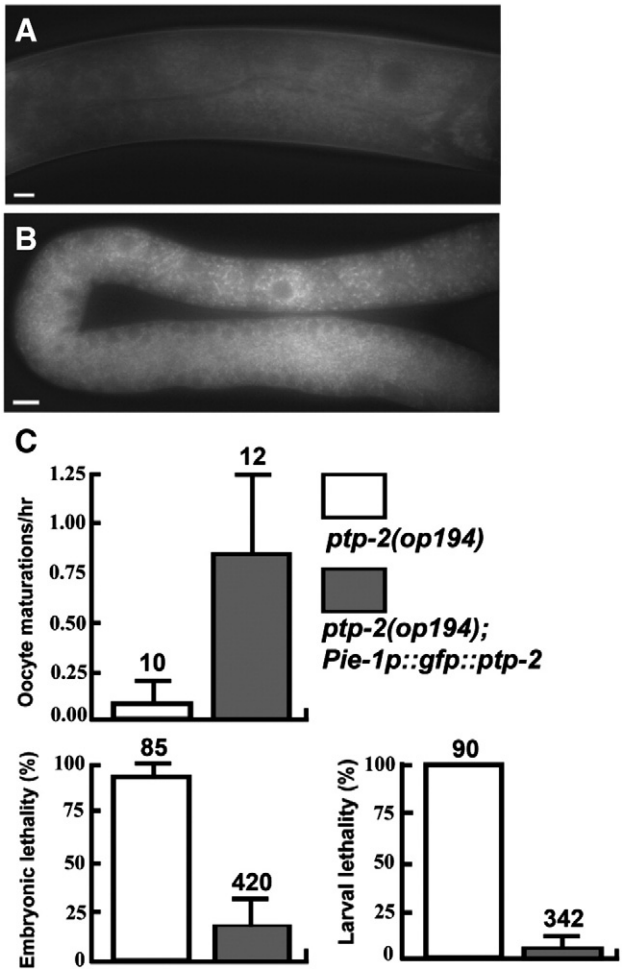

Fig. 6. Germline GFP::PTP-2 expression rescues *ptp-2(op194)* phenotypes. (A, B) GFP::PTP-2 expression, driven with the *pie-1* promoter, is faint, but detectable in the germ line of adult hermaphrodites (A). GFP is observed throughout the germ cell and oocyte cytoplasm, but not in the nucleus or at the cell surface. In dissected gonads, GFP appears to localize to vesicles in the oocytes (B). Gonad orientation is with spermatheca to the right. (C) The transgene partially rescues the oocyte maturation rate, embryonic lethality, and larval lethality defects of *ptp-2(op194)* mutants. N is shown above error bars, which represent standard deviation. Scale bars, 10 μm.

compared to wild-type gonads (Fig. 7A and D). Similar results are observed in *sod-1* RNAi gonads (Fig. 7D). *C. elegans* contains a second Cu/Zn superoxide dismutase called *sod-5* that can partially compensate for *sod-1* loss (Yanase et al., 2009). Silencing of both *sod-1* and *sod-5* by RNAi results in higher dpMPK-1 levels than *sod-1* RNAi alone and wild-type controls (Fig. 7D). The oocyte maturation rate of *sod-1(tm776)* hermaphrodites is similar to the wild-type rate, indicating that elevated MPK-1 activity does not cause abnormally high maturation rates (Table 1, compare line 23 to line 1). These results indicate that SOD-1 negatively regulates oocyte MPK-1 phosphorylation. To investigate the genetic relationship between *sod-1* and *mpk-1*, we examined *sod-1* RNAi *ptp-2(op194)* gonads. In contrast to *ptp-2(op194)* gonads (Fig. 4B), MPK-1 phosphorylation is detectable in *sod-1* RNAi *ptp-2(op194)* and *sod-1 sod-5* double RNAi *ptp-2(op194)* gonads (Fig. 7B and C). Therefore, *sod-1* inhibits MPK-1 phosphorylation downstream of *ptp-2* or in a parallel pathway. Taken together, the data support the hypothesis that ROS are downstream secondary messengers involved in MSP signaling.

Sperm/MSP stimulate ROS production

Paraquat generates intracellular ROS that cause concentration-dependent toxicity depending on endogenous ROS and superoxide dismutase activity. To test whether sperm influence ROS levels, we incubated unmated females and wild-type hermaphrodites with increasing concentrations of paraquat. Unmated females are more resistant than wild-type hermaphrodites to paraquat-induced lethality (Fig. 8A). Therefore, sperm presence causes increased ROS, decreased superoxide dismutase activity, or a combination of both. If MSP acts solely to inhibit SOD-1 activity, then *sod-1* loss in unmated females should cause increased MPK-1 phosphorylation or oocyte maturation. Oocyte MPK-1 phosphorylation is not detected in unmated *sod-1* mutant females (Fig. 7D) and the oocyte maturation rate of unmated *sod-1(tm776); fog-2(q71)* females is not significantly different than unmated control females (Table 1, compare line 24 to line 5). These results suggest that MSP induces ROS production. To examine ROS levels, we used the ROS indicator 2,7-dichlorodihydro-fluorescein-diacetate (H_2-DCF-DA), a nonfluorescent dye that becomes trapped in cells and fluoresces following ROS oxidation. In dissected gonads, the most proximal oocytes of wild-type hermaphrodites have increased fluorescence compared to unmated *fog-2(q71)* females (Fig. 8B–E). The fluorescence pattern is compartmentalized within individual oocytes, resembling the MPK-1 phosphorylation pattern. Similar results are observed in live animals incubated with H_2-DCF-DA for several hours, except the staining frequency is much lower, possibly due to poor dye penetration into the gonad (Fig. 8F and G). *sod-1(tm776)* mutant gonads incubated with H_2-DCF-DA often contained more fluorescent oocytes than wild-type gonads (data not shown). These results support the model that MSP induces ROS production to augment MPK-1 phosphorylation.

ROS such as superoxide are a byproduct of mitochondrial respiration, raising the possibility that MSP stimulates respiration to increase ROS levels. We tested this possibility using Mitotracker CMXRos, a red-fluorescent dye that stains mitochondria undergoing respiration. CMXRos accumulation is dependent upon membrane potential generated from pumping hydrogen ions across the inner membrane during electron transport (Pendergrass et al., 2004; Sherwood et al., 2005). In dissected gonads, mitochondria in the most proximal oocytes and sperm often stain more intensely with Mitotracker CMXRos than those in developing oocytes or germ cells (Fig. 9A and not shown). In unmated *fog-2(q71)* females, oocyte mitochondrial fluorescence is less intense and uniform throughout the proximal gonad (Fig. 9B). These data are consistent with the possibility that MSP promotes increased respiration in the most proximal oocytes. Next, we measured oxygen consumption in wild-type hermaphrodites containing sperm and unmated *fog-2(q71)* females. Wild-type hermaphrodites consume more oxygen than unmated females when the data are normalized to worm number ($P = 0.02$; Fig. 9C). However, there is no significant difference when the data are normalized to protein content (Fig. 9D), indicating that females contain less protein. Unmated females have more oocytes than wild-type hermaphrodites, but no sperm or embryos. The increased oxygen consumption rates in the wild type could, therefore, be due to oocytes, sperm, embryos, or a combination. A previous study has shown that the presence of both sperm and oocytes, but not embryos causes anoxia sensitivity, a result consistent with our oxygen consumption data normalized to worm number (Mendenhall et al., 2009). Taken together, most data are consistent with MSP promoting mitochondrial respiration to increase cytosolic ROS levels and MPK-1 phosphorylation. However, the mitochondrial respiration component needs further study to be definitive.

Discussion

MSP regulates a complex network of signaling cascades in sheath cells and oocytes to induce sheath contraction and oocyte maturation. In this study, we show that MSP antagonizes sheath/oocyte gap junctional communication to activate an oocyte cascade comprised of PTP-2 Shp, GAP-1 and GAP-2 RasGAPs, LET-60 Ras, and MPK-1 MAPK. We propose that PTP-2 associates with the cytoplasmic domain of an

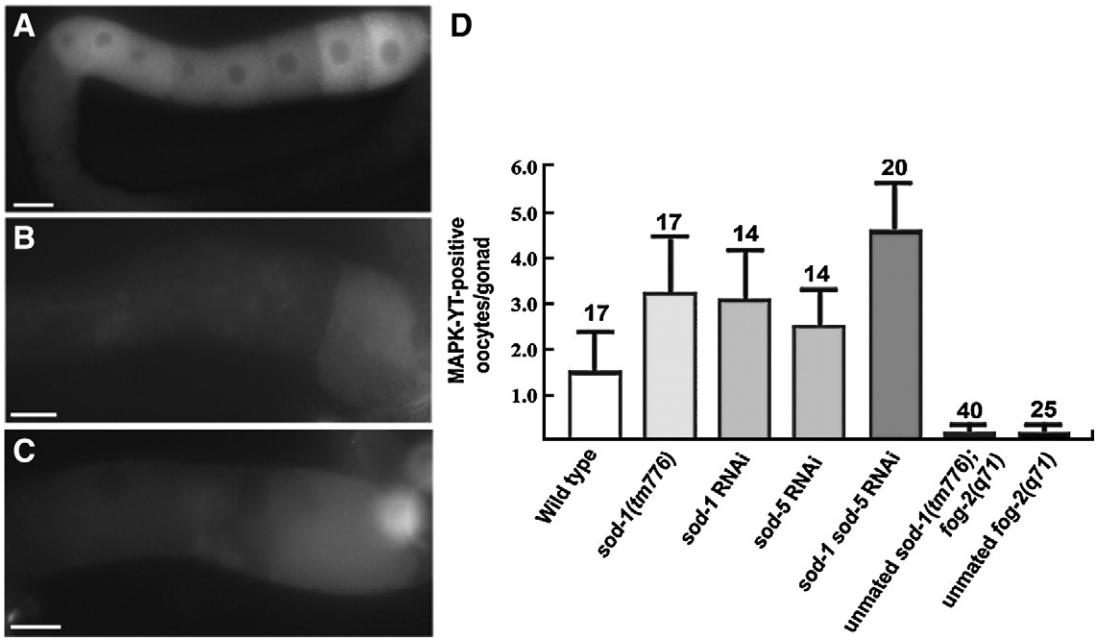

Fig. 7. Cu/Zn superoxide dismutase activity antagonizes oocyte MPK-1 phosphorylation. (A) Multiple oocytes in *sod-1(tm776)* hermaphrodite gonads contain phosphorylated MPK-1, detected using the MAPK-YT antibody. (B, C) In *ptp-2(op194)* mutants, *sod-1* RNAi (B) and *sod-1 sod-5* double RNAi (C) partially rescue the MPK-1 phosphorylation defect. Phosphorylated MPK-1 is not observed in *ptp-2(op194)* gonads (see Fig. 3B and H). Gonad orientation is with spermatheca to the right. (D) Quantification of oocyte MPK-1 phosphorylation levels in proximal gonads. N is shown above error bars, which represent standard deviation. Scale bars, 20 μm.

unknown receptor in an oocyte vesicular compartment to inhibit RasGAP activity, resulting in sustained MPK-1 activation essential for high oocyte maturation rates. In a second mechanism, MSP stimulates production of reactive oxygen species, which act as second messengers to augment MPK-1 phosphorylation. The Cu/Zn superoxide dismutases SOD-1 acts downstream of *ptp-2* or in a parallel pathway to attenuate MPK-1 phosphorylation. Evidence for this model is discussed in the following paragraphs.

We show that PTP-2 is required to promote high oocyte maturation rates in response to MSP. *ptp-2* null mutant gonads initiate sheath contraction, oocyte histone phosphorylation, and oocyte growth pathways. However, MPK-1 fails to become fully activated in the proximal oocytes. Genetic data support a model similar to one proposed for *Drosophila* CSW. During embryonic development, the receptor tyrosine kinase Torso promotes sustained activation of the MAPK cascade to specify terminal structures (Cleghon et al., 1998). CSW physically associates with torso by binding to pY630. CSW recruitment promotes the dephosphorylation of pY918, a RasGAP binding site. The loss of local RasGAP activity promotes sustained Ras activation. During *C. elegans* oocyte maturation, MSP stimulates the phosphorylation and activation of oocyte MPK-1. MPK-1 phosphorylation levels are low in *ptp-2* null mutant oocytes, despite the presence of MSP and cell surface MSP receptors. A gain-of-function mutation in *let-60* Ras or loss of multiple RasGAPs suppresses the *ptp-2* mutant oocyte maturation rate defect, as well as the embryonic and larval lethality. Increased

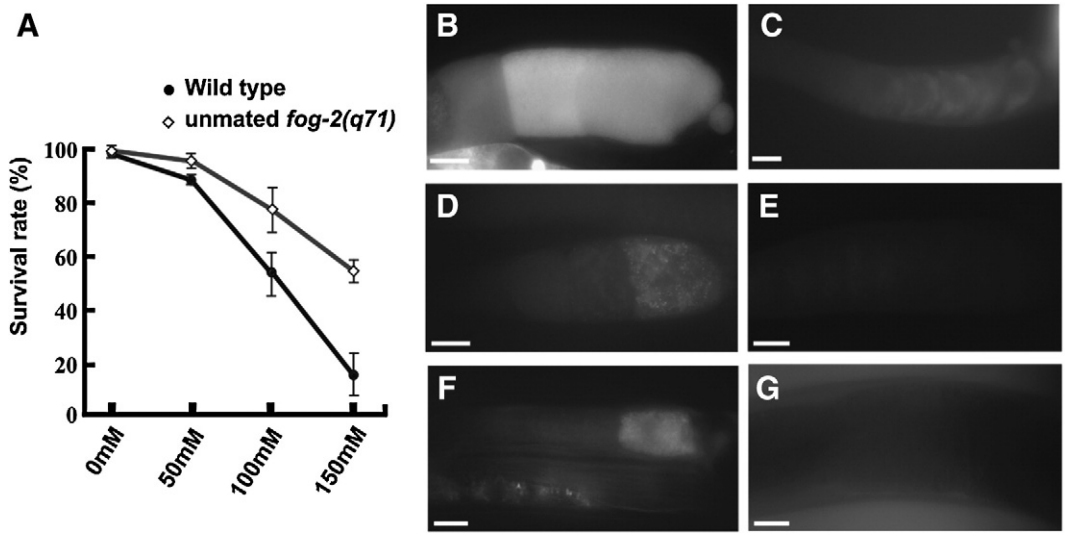

Fig. 8. Sperm promote increased reactive oxygen species levels. (A) Unmated females are more resistant than wild-type hermaphrodites to paraquat-induced lethality. Paraquat generates intracellular superoxide that becomes toxic depending on endogenous ROS levels and superoxide dismutase activity. (B–G) The ROS indicator H2-DCF-DA shows enhanced fluorescence in wild-type dissected gonads (B, D) and live animals (F) compared to unmated *fog-2(q71)* female dissected gonads (C, E) and live animals (G). Dissected gonads in panels D and E were lightly fixed prior to mounting, causing a reduction in fluorescent intensity (see Materials and methods). Gonad orientation is with spermatheca to the right. Scale bars, 20 μm.

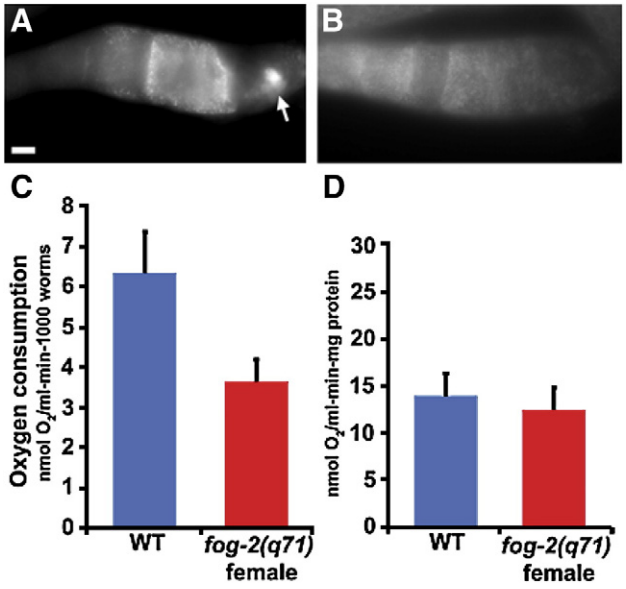

Fig. 9. Oocyte mitochondrial function in the presence and absence of sperm. (A, B) Dissected proximal wild-type (A) and unmated *fog-2(q71)* female (B) gonads stained with Mitotracker CMXRos. Gonad orientation is with spermatheca to the right. The bright fluorescence in the wild-type spermatheca (panel A) is sperm mitochondria (arrow). Scale bar, 20μm. (C, D) Oxygen consumption rates in wild-type hermaphrodites (WT) and unmated *fog-2(q71)* females normalized to worm number (C) and protein content (D). The *P* values calculated using a Student's *t*-test are 0.02 for panel C and 0.5 for panel D.

MPK-1 phosphorylation is detected in these suppressed mutants, although the levels are reduced compared to the wild type. The results suggest that a small increase in Ras activity is sufficient to restore oocyte maturation rates and viability in *ptp-2* mutants. Our data are consistent with those of Lee et al., who showed that a genetic reduction in *mpk-1* activity delays oocyte maturation (Lee et al., 2007). *ptp-2* mutants do not have the pachytene arrest phenotype observed in *let-60* and *mpk-1* null mutants (Church et al., 1995; Lee et al., 2007), although meiotic progression may be delayed. Maternal *ptp-2* could be sufficient to promote pachytene exit or alternatively, *ptp-2* may not be required at this stage. *ptp-2* null mutant oocytes are large and resemble those seen in hypomorphic *mpk-1* mutant strains. Therefore, it seems likely that MPK-1 activity is reduced, but not eliminated in *ptp-2* mutants.

MPK-1 activation is a late event in the MSP signaling response, occurring approximately 30–45 min after the microinjection of extracellular MSP (Han et al., 2009; Miller et al., 2001). This delay suggests that the PTP-2/LET-60/MPK-1 cascade is downstream in the oocyte maturation signaling hierarchy. Genetic and transgenic studies provide additional support. Phosphorylated MPK-1 is uniformly distributed throughout the oocyte cytoplasm and similar to the PTP-2 subcellular localization, except that PTP-2 appears to localize to vesicles. Driving GFP::PTP-2 expression specifically in the germ line partially rescues the oocyte maturation and MPK-1 activation defects, as well as embryonic lethality of *ptp-2* null mutants. The incomplete rescue could be due to insufficient germline expression levels, the N-terminal GFP interfering with PTP-2 function, or lack of sheath PTP-2 expression. In germ cells and oocytes, GFP::PTP-2 localizes to the cytoplasm, but not at the cell surface or in the nucleus. Genetic analyses are consistent with *ptp-2* acting downstream of the MSP receptor *vab-1*, the CaMKII *unc-43*, and components of sheath/oocyte gap junctions. *ptp-2's* genetic relationship with sheath/oocyte gap junctions contrasts with that of *gsa-1*, which is required in the sheath cells (Govindan et al., 2006; Govindan et al., 2009). The data support the model that sheath $G_{\alpha s}$-adenylate cyclase signaling functions upstream of sheath/oocyte gap junctions to regulate the PTP-2/LET-60/MPK-1 cascade. It is not well understood how MSP couples to GSA-1 and how gap junctions couple to PTP-2.

Ras gain of function females lacking sperm have low oocyte maturation rates and MPK-1 phosphorylation levels, suggesting that MSP regulates additional mechanisms important for MPK-1 activation. Paraquat and ROS indicator studies are consistent with MSP increasing oocyte ROS levels. Genetic studies using the Cu/Zn superoxide dismutases, which function to breakdown ROS in the cytoplasm, add further support. SOD-1 and SOD-5 act together to negatively regulate MSP-induced MPK-1 phosphorylation downstream of *ptp-2* or in a parallel pathway. Cu/Zn superoxide dismutase activity is not required in the absence of sperm. ROS are rapidly diffusing second messengers known to positively influence the MAPK cascade in cultured mammalian cells (Abe et al., 2000; Aikawa et al., 1997; Secondo et al., 2008). Rapid diffusion could partially explain how MPK-1 becomes phosphorylated throughout the oocyte cytosol in response to MSP. The mechanism by which MSP induces ROS may involve increased oocyte mitochondrial respiration, generating energy for oocyte maturation and early embryogenesis. ROS are formed during mitochondrial electron transport when oxygen is incompletely reduced. MitoTracker CMXRos and oxygen consumption assays normalized to worm number are consistent with increased oxidative respiration. Additional support comes from previous studies showing that the presence of both sperm and oocytes, but not embryos makes hermaphrodites more sensitive to anoxia (Mendenhall et al., 2009). Cells undergoing high rates of mitochondrial respiration are likely to be more sensitive to anoxia. However, oxygen consumption assays normalized to protein content do not support a role for MSP in mitochondrial respiration. It is possible that sperm presence promotes increased respiration and protein synthesis. Alternatively, increased oxygen consumption rates in hermaphrodites could be due to embryos. Further studies are necessary to understand the relationship between MSP domains and mitochondrial function.

Shp class phosphatases are characterized by the presence of two N-terminal SH2 domains that often bind to phosphotyrosines on receptor intracellular regions (Neel et al., 2003). *Drosophila* CSW acts downstream of the receptor tyrosine kinases Torso, Sevenless, Deranged, Breathless, and Heartless (Allard et al., 1996; Perkins et al., 1992, 1996). In *C. elegans*, the MSP receptor VAB-1 is an Eph receptor protein-tyrosine kinase that negatively regulates MPK-1 activation (Miller et al., 2003). Most data do not support the model that VAB-1 and PTP-2 interact. PTP-2 does not appear to localize to the cell surface, contrasting with VAB-1 localization (Cheng et al., 2008; Miller et al., 2003). Furthermore, genetic studies are consistent with *ptp-2* acting downstream of *unc-43* and sheath/oocyte gap junctions. If there is an interaction between VAB-1 and PTP-2, the mechanism is likely to be transient and involve additional receptors. A more likely scenario is that PTP-2 interacts with an unidentified receptor localizing to endosomes or another intracellular compartment in oocytes. In cultured mammalian cells, the localization of Ras and Erk to various intracellular compartments, including endosomes, is mechanistically linked to sustained MAPK signaling (Bivona and Philips, 2003; Mor and Philips, 2006).

MAPK activation is a key step in vertebrate oocyte maturation, although the regulatory mechanisms and site of action are still debated (Liang et al., 2007). In *Xenopus* oocytes, progesterone-induced oocyte maturation is accompanied by MAPK activation. Constitutively active MAPK promotes oocyte maturation in the absence of progesterone and chemically inhibiting MAPK prevents maturation (Grigorescu et al., 1994; Posada and Cooper, 1992). MAPK activation is thought to be mediated by the proto-oncogene MOS, a vertebrate germ cell-specific kinase that phosphorylates MAP Kinase Kinase (Liang et al., 2007; Seger and Krebs, 1995). However, MOS inactivation by morpholinos does not prevent oocyte maturation (Dupre et al., 2002). In mice, deletion of *mos* or *erk1* does not prevent luteinizing hormone-induced oocyte maturation, but deletion of *erk1*

and *erk2* in granulosa cells does (Fan et al., 2009; Hashimoto et al., 1994; Liang et al., 2007). Thus, MAPK activity is essential in the granulosa cells, but probably not in the oocytes. Whether Shps play a role in vertebrate oocyte maturation is not known. *C. elegans* MPK-1 activation does not involve MOS. Although MPK-1 activation is observed in oocytes and surrounding sheath cells, the essential role appears to be in oocytes. These species-specific differences in MAPK regulation may be due to differences in the maturation-inducing hormones and their transduction mechanisms.

There is accumulating evidence that the MSP domain has an evolutionarily conserved signaling function mediated by Eph receptors and other receptors. The human VAPB MSP domain is found in blood serum, possesses extracellular signaling and receptor binding activities in *C. elegans* gonads, and can bind to the mouse EphA4 receptor (Tsuda et al., 2008). A P56S substitution in the human VAPB MSP domain is associated with ALS, although the pathological mechanism is not understood (Nishimura et al., 2004). P56S acts as a dominant negative mutation in multiple model systems and prevents VAP MSP domain secretion in fly cells (Ratnaparkhi et al., 2008; Teuling et al., 2007; Tsuda et al., 2008). Dominant mutations in *sod1* are also associated with ALS and these are gain of function (Rosen et al., 1993; Rothstein, 2009). Our results support the model that MSP and SOD-1 act antagonistically to control ROS and MPK-1 signaling. Therefore, it is possible that MSP domain proteins and Cu/Zn superoxide dismutases are components of an evolutionarily ancient signaling mechanism important for human motor neuron survival.

Materials and methods

C. elegans genetics and strains

C. elegans variety Bristol, strain N2 is the wild-type strain. Cultures were grown on NGM plates with NA22 bacteria as the food source (Brenner, 1974). *fog-2(q71)* strains (Schedl and Kimble, 1988) were maintained as male/female stocks, while *fog-3(q443)* strains (Ellis and Kimble, 1995) were balanced with the translocation *hT2(qIs48)I*. Strain construction and marker scoring were done as previously described using PCR and phenotypic analyses (Miller et al., 2003). Genes, alleles, and balancer chromosomes are described in WormBase (http://www.wormbase.org). The strains and genetic markers used or generated were as follows: WS841 [*ptp-2(op194) unc-4(e120)/mIn1II; him-5(e1490) V*] (Gutch et al., 1998), DG1743 [*fog-3(q443)/hT2(qIs48)I*] (Miller et al., 2003), MT1092 [*unc-43(n498)IV*] (Reiner et al., 1999), CZ337 [*vab-1(dx31)II*] (George et al., 1998), HT1593 [*unc-119 (ed3)III*] (Praitis et al., 2001), MT2124 [*let-60(n1046)IV*], AH12 [*gap-1(ga133)X*] (Hajnal et al., 1997), JN147 [*gap-2(tm748)X*], XM1011 [*inx-22(tm1661)I*] (Whitten and Miller, 2007), FX776 [*sod-1(tm776)II*] (Yanase et al., 2009), CB4108 [*fog-2(q71)V*], [*ptp-2 (op194) unc-4(e120)/mIn1II; fog-2(q71)V*], [*fog-3(q443)/hT2(qIs48)I; let-60(n1046)IV*], [*inx-22(tm1661)I; ptp-2(op194) unc-4(e120)/mIn1II*], [*ptp-2(op194) unc-4(e120)/mIn1II; let-60(n1046)IV*], [*ptp-2 (op194) unc-4(e120)/mIn1II; unc-43(n498)IV*], [*ptp-2(op194) unc-4 (e120)/mIn1II; gap-1(ga133)X; gap-2(tm748)X*], [*ptp-2(op194) unc-4 (e120)/mIn1II; gap-1(ga133)X*], [*ptp-2(op194) unc-4(e120)/mIn1II; gap-2(tm748)X*], [*ptp-2(op194) unc-4(e120)/mIn1II; Ex [pie-1p::gfp::ptp-2 + unc-119(+)], and* [*sod-1(tm776); fog-2(q71)*]. The *sod-1 (tm776)* mutation was backcrossed to the wild-type four times.

Phenotypic analysis and rate determination

Oocyte meiotic maturation and ovarian sheath contraction were analyzed in anesthetized animals (0.1% tricaine and 0.01% tetramisole in M9 buffer) on 2% agarose pads as previously described (McCarter et al., 1999). A Zeiss Axioskop 2 plus, MRM Axiocam Hi-Res digital camera, and PC computer were used to observe and record images. DAPI staining of dissected gonads was used for evaluating oocyte meiotic progression. Oocyte maturation and sheath contraction were monitored for each strain by direct observation using DIC optics. For adult hermaphrodites and females, basal sheath contraction rates were measured as previously described (McCarter et al., 1999; Miller et al., 2003). Oocyte maturation rates were determined by monitoring oocyte ovulation in isolated animals on seeded plates for 1.5 to 24 h, which was consistent with direct observation by DIC microscopy. Because food is required for high maturation rates, monitoring animals on seeded plates is optimal for accurate quantification over time periods > 90 min. Tables 1 and 2 show average oocyte maturation or sheath contraction rates ± standard deviation. To test for significance, a two sample *t*-test was used.

RNA-mediated interference

RNAi was performed by the feeding and soaking methods (Timmons et al., 2001; Timmons and Fire, 1998). RNAi HT115 bacterial feeding strains are from the genome-wide library (Kamath et al., 2003). Each clone was sequenced for confirmation.

Transgenics

For generating transgenic *C. elegans*, 5 kb of genomic DNA upstream of the *ptp-2* translational start site was inserted into pPD95.81 upstream of GFP. The primers 5'-CGGGGATCCCGCTTGCATGAAACATGAAATTGGTGG-3' and 5'-TCTACCGGTACTTCACCATTCACGCGGTAATAG-3' were used for PCR amplification of genomic DNA. The plasmid (90 μg/ml) was mixed with pRF4 [rol-6(d)] (90 μg/ml) and injected into the gonads of young adult hermaphrodites. Transgenic progeny were selected based on the roller phenotype. Multiple independent lines for each transgene were analyzed. To generate the *pie-1p::gfp::ptp-2* transgene, the *ptp-2* ORF was cloned into pDONR201 (Invitrogen, Carlsbad, CA) before recombining into pID3.01B, which contains the *pie-1* promoter upstream of *gfp* and the cloning site. This construct was sequenced and transformed into *unc-119(ed3)* hermaphrodites by microparticle bombardment (Praitis et al., 2001). Multiple transgenic lines were generated. One transgenic line with ~95% *unc-119*(+) animals and visible GFP expression was crossed into *ptp-2(op194) unc-4(e120)/mIn1II* hermaphrodites. The genotype was confirmed by PCR. The resulting *ptp-2(op194) unc-4 (e120); Piep::gfp::ptp-2 + unc-119(+)* strain was homozygous viable, contrasting with *ptp-2(op194) unc-4(e120)* mutants. GFP expression in this line was faint, but detectable.

Immunocytochemistry and GFP imaging

Monoclonal MAPK-YT (Sigma), anti-phosphohistone H3 (Upstate Biotechnology, Waltham, MA), anti-NOP1 (Encor Biotech, Alachua, FL) antibodies were incubated with dissected gonads as previously described (Burrows et al., 2006; Miller et al., 2001). Dissected gonads were fixed in 2% neutral-buffered paraformaldehyde at 4 °C overnight, washed in PBT, blocked with 1 mg/ml BSA for 2 h, and then incubated with the antibodies for 4 h at room temperature. The concentrations were as follows: MAPK-YT (1:2000), anti-phospho-histone H3 (1:500), and anti-Nop1 (1:500). Anti-mouse or anti-rabbit FITC-conjugated secondary antibodies were used for detection. DAPI was used to visualize DNA. For evaluating GFP expression of transgenic *pie-1p::gfp::ptp-2* strains, animals were kept in the dark for 24 h prior to visualization.

MSP microinjection and binding

Recombinant 6His-MSP was expressed and purified under native conditions as previously described (Miller et al., 2001). MSP concentrations were determined by the BCA protein assay. MSP or M9 buffer alone

was microinjected through the vulva using a Zeiss Axiovert 200 microscope, hydraulic fine type micromanipulator, and Narishige IM-30 microinjector (Corrigan et al., 2005; Tsuda et al., 2008). To evaluate MSP binding, recombinant 6His-MSP was conjugated to NHS-Fluorescein and purified (Miller et al., 2003). Binding assays were conducted as previously described (Miller et al., 2003; Tsuda et al., 2008). MSP-FITC is biologically active and binding is specific.

Paraquat resistance and reactive oxygen species

Resistance to paraquat was determined as described previously with slight modification (An and Blackwell, 2003; Li et al., 2008). Forty one-day adult wild-type hermaphrodites or unmated *fog-2(q71)* females were placed in 200 µl of M9 buffer containing 0, 50, 100, or 150 mM paraquat for 24 h at 20 °C. After the incubation, 0.5 ml of M9 was added and the worms were transferred to NGM plates and examined for survival. Worms that failed to respond to gentle prodding were scored as dead. Each genotype was analyzed in triplicate.

Intracellular ROS levels were determined using the membrane-permeable nonfluorescent dye 2,7-dichlorodihydrofluorescein-diacetate (H_2-DCF-DA) (Anaspec, Fremont, CA). After entry into cells, H_2-DCF-DA is converted to membrane-impermeable HDCF. In the presence of ROS, HDCF is oxidized to fluorescent 2,7-dichlorofluorescein (DCF). Dissected adult gonads were soaked in 50 µM H_2-DCF-DA buffer for 10 min and mounted on agarose pads without fixation using Vaseline to prevent the coverslip from crushing the gonads. Unfixed gonads mounted under a coverslip are difficult to image, limiting the number of samples that can be analyzed. To help circumvent this issue, we lightly fixed the gonads in 1% neutral-buffered paraformaldehyde for 5 min before mounting. Fixation decreased the fluorescent intensity, but facilitated analysis of larger gonad numbers. In addition, we soaked live worms in H_2-DCF-DA for 7 h, anesthetized them, and mounted them for microscopy. In live animals, fluorescent oocytes were sometimes observed in wild-type hermaphrodites, but not unmated females. The lower frequency in live hermaphrodites relative to dissected gonads might be due to poor dye penetration into the gonad. Fluorescence was monitored using a Zeiss Axioskop 2 microscope equipped with fluorescence and a GFP filter. Hermaphrodite and unmated female gonads were analyzed in the same solution and independently.

Mitotracker CMXRos and oxygen consumption

Dissected worm gonads were incubated in 50nM MitoTracker Red CMXRos (Molecular Probes, Inc., Eugene, OR) and placed in dark place at room temperature for 10 min. Gonads were lightly fixed in 1% neutral-buffered paraformaldehyde for 5 min before mounting. Hermaphrodite and unmated female gonads were analyzed in the same solution and independently. Oxygen consumption rates were measured as previously described using the oxygraph system (Hansatech, UK) with slight modifications (Braeckman et al., 2002). Synchronized wild-type and unmated *fog-2(q71)* female worms were grown to L4 stage, transferred to new NGM plates, and incubated for an additional 24 h at 20 °C. 1000 1 day old adult worms were individually picked and collected into 1 ml M9 buffer prepared at 20 °C. Worms were incubated for 40 min at 20 °C to remove the intestinal bacteria and washed five times using M9 buffer. 1 ml M9 with 1000 worms was placed into the chamber equipped with a S1 Clark type polarographic oxygen electrode disc. The chamber was maintained at 20 °C using a constant-temperature circulating water bath and the oxygen concentration was measured for at least 10 min. Worms were carefully collected from the chamber for protein quantification. Rates were normalized to either total protein content or the number of worms. We performed at least three independent measurements per strain.

Acknowledgments

We thank Pauline Cottee and Wes Edmonds for comments on the manuscript. Some strains were provided by the *Caenorhabditis* Genetics Center, which is funded by the NIH. Financial support for this study came from an American Cancer Society Research Scholars Grant to M.A.M. (RSG-06-151-01-DDC). The *sod-1(tm776)* strain was created by the Japanese National Bioresource Project, which is supported by the Ministry of Education, Culture, Science, Sports and Technology.

Appendix A. Supplementary data

Supplementary data associated with this article can be found, in the online version, at doi:10.1016/j.ydbio.2010.03.026.

References

Abe, J., Okuda, M., Huang, Q., Yoshizumi, M., Berk, B.C., 2000. Reactive oxygen species activate p90 ribosomal S6 kinase via Fyn and Ras. J. Biol. Chem. 275, 1739–1748.
Aikawa, R., Komuro, I., Yamazaki, T., Zou, Y., Kudoh, S., Tanaka, M., Shiojima, I., Hiroi, Y., Yazaki, Y., 1997. Oxidative stress activates extracellular signal-regulated kinases through Src and Ras in cultured cardiac myocytes of neonatal rats. J. Clin. Invest. 100, 1813–1821.
Allard, J.D., Chang, H.C., Herbst, R., McNeill, H., Simon, M.A., 1996. The SH2-containing tyrosine phosphatase corkscrew is required during signaling by sevenless, Ras1 and Raf. Development 122, 1137–1146.
An, J.H., Blackwell, T.K., 2003. SKN-1 links *C. elegans* mesendodermal specification to a conserved oxidative stress response. Genes Dev. 17, 1882–1893.
Aris, J.P., Blobel, G., 1989. Yeast nuclear envelope proteins cross react with an antibody against mammalian pore complex proteins. J. Cell Biol. 108, 2059–2067.
Bivona, T.G., Philips, M.R., 2003. Ras pathway signaling on endomembranes. Curr. Opin. Cell Biol. 15, 136–142.
Bottino, D., Mogilner, A., Roberts, T., Stewart, M., Oster, G., 2002. How nematode sperm crawl. J. Cell Sci. 115, 367–384.
Braeckman, B.P., Houthoofd, K., De Vreese, A., Vanfleteren, J.R., 2002. Assaying metabolic activity in ageing *Caenorhabditis elegans*. Mech. Ageing Dev. 123, 105–119.
Brenner, S., 1974. The genetics of *Caenorhabditis elegans*. Genetics 77, 71–94.
Bullock, T.L., Roberts, T.M., Stewart, M., 1996. 2.5 A resolution crystal structure of the motile major sperm protein (MSP) of Ascaris suum. J. Mol. Biol. 263, 284–296.
Burrows, A.E., Sceurman, B.K., Kosinski, M.E., Richie, C.T., Sadler, P.L., Schumacher, J.M., Golden, A., 2006. The *C. elegans* Myt1 ortholog is required for the proper timing of oocyte maturation. Development 133, 697–709.
Cheng, H., Govindan, J.A., Greenstein, D., 2008. Regulated trafficking of the MSP/Eph receptor during oocyte meiotic maturation in *C. elegans*. Curr. Biol. 18, 705–714.
Church, D.L., Guan, K.L., Lambie, E.J., 1995. Three genes of the MAP kinase cascade, mek-2, mpk-1/sur-1 and let-60 ras, are required for meiotic cell cycle progression in *Caenorhabditis elegans*. Development 121, 2525–2535.
Cleghon, V., Feldmann, P., Ghiglione, C., Copeland, T.D., Perrimon, N., Hughes, D.A., Morrison, D.K., 1998. Opposing actions of CSW and RasGAP modulate the strength of Torso RTK signaling in the *Drosophila* terminal pathway. Mol. Cell 2, 719–727.
Corrigan, C., Subramanian, R., Miller, M.A., 2005. Eph and NMDA receptors control Ca2 +/calmodulin-dependent protein kinase II activation during *C. elegans* oocyte meiotic maturation. Development 132, 5225–5237.
Dupre, A., Jessus, C., Ozon, R., Haccard, O., 2002. Mos is not required for the initiation of meiotic maturation in *Xenopus* oocytes. EMBO J. 21, 4026–4036.
Ellis, R.E., Kimble, J., 1995. The fog-3 gene and regulation of cell fate in the germ line of *Caenorhabditis elegans*. Genetics 139, 561–577.
Fan, H.Y., Liu, Z., Shimada, M., Sterneck, E., Johnson, P.F., Hedrick, S.M., Richards, J.S., 2009. MAPK3/1 (ERK1/2) in ovarian granulosa cells are essential for female fertility. Science 324, 938–941.
Feng, G.S., 1999. Shp-2 tyrosine phosphatase: signaling one cell or many. Exp. Cell Res. 253, 47–54.
George, S.E., Simokat, K., Hardin, J., Chisholm, A.D., 1998. The VAB-1 Eph receptor tyrosine kinase functions in neural and epithelial morphogenesis in *C. elegans*. Cell 92, 633–643.
Govindan, J.A., Cheng, H., Harris, J.E., Greenstein, D., 2006. Galphao/i and Galphas signaling function in parallel with the MSP/Eph receptor to control meiotic diapause in *C. elegans*. Curr. Biol. 16, 1257–1268.
Govindan, J.A., Nadarajan, S., Kim, S., Starich, T.A., Greenstein, D., 2009. Somatic cAMP signaling regulates MSP-dependent oocyte growth and meiotic maturation in *C. elegans*. Development 136, 2211–2221.
Greenstein, D., 2005. Control of oocyte meiotic maturation and fertilization. WormBook 1–12.
Grigorescu, F., Baccara, M.T., Rouard, M., Renard, E., 1994. Insulin and IGF-1 signaling in oocyte maturation. Horm. Res. 42, 55–61.
Gutch, M.J., Flint, A.J., Keller, J., Tonks, N.K., Hengartner, M.O., 1998. The *Caenorhabditis elegans* SH2 domain-containing protein tyrosine phosphatase PTP-2 participates in signal transduction during oogenesis and vulval development. Genes Dev. 12, 571–585.

Hajnal, A., Whitfield, C.W., Kim, S.K., 1997. Inhibition of *Caenorhabditis elegans* vulval induction by gap-1 and by let-23 receptor tyrosine kinase. Genes Dev. 11, 2715–2728.

Han, S.M., Cottee, P.A., Miller, M.A., 2009. Sperm and oocyte communication mechanisms controlling *C. elegans* fertility. Dev. Dyn. (December 23, Electronic publication ahead of print).

Harris, J.E., Govindan, J.A., Yamamoto, I., Schwartz, J., Kaverina, I., Greenstein, D., 2006. Major sperm protein signaling promotes oocyte microtubule reorganization prior to fertilization in *Caenorhabditis elegans*. Dev. Biol. 299, 105–121.

Hashimoto, N., Watanabe, N., Furuta, Y., Tamemoto, H., Sagata, N., Yokoyama, M., Okazaki, K., Nagayoshi, M., Takeda, N., Ikawa, Y., et al., 1994. Parthenogenetic activation of oocytes in c-mos-deficient mice. Nature 370, 68–71.

Henriquez, R., Blobel, G., Aris, J.P., 1990. Isolation and sequencing of NOP1. A yeast gene encoding a nucleolar protein homologous to a human autoimmune antigen. J. Biol. Chem. 265, 2209–2215.

Hsu, J.Y., Sun, Z.W., Li, X., Reuben, M., Tatchell, K., Bishop, D.K., Grushcow, J.M., Brame, C. J., Caldwell, J.A., Hunt, D.F., Lin, R., Smith, M.M., Allis, C.D., 2000. Mitotic phosphorylation of histone H3 is governed by Ipl1/aurora kinase and Glc7/PP1 phosphatase in budding yeast and nematodes. Cell 102, 279–291.

Hsu, V., Zobel, C.L., Lambie, E.J., Schedl, T., Kornfeld, K., 2002. *Caenorhabditis elegans* lin-45 raf is essential for larval viability, fertility and the induction of vulval cell fates. Genetics 160, 481–492.

Jud, M.C., Czerwinski, M.J., Wood, M.P., Young, R.A., Gallo, C.M., Bickel, J.S., Petty, E.L., Mason, J.M., Little, B.A., Padilla, P.A., Schisa, J.A., 2008. Large P body-like RNPs form in *C. elegans* oocytes in response to arrested ovulation, heat shock, osmotic stress, and anoxia and are regulated by the major sperm protein pathway. Dev. Biol. 318, 38–51.

Kamath, R.S., Fraser, A.G., Dong, Y., Poulin, G., Durbin, R., Gotta, M., Kanapin, A., Le Bot, N., Moreno, S., Sohrmann, M., Welchman, D.P., Zipperlen, P., Ahringer, J., 2003. Systematic functional analysis of the *Caenorhabditis elegans* genome using RNAi. Nature 421, 231–237.

Klass, M.R., Hirsh, D., 1981. Sperm isolation and biochemical analysis of the major sperm protein from *C. elegans*. Dev. Biol. 84, 299–312.

Kosinski, M., McDonald, K., Schwartz, J., Yamamoto, I., Greenstein, D., 2005. *C. elegans* sperm bud vesicles to deliver a meiotic maturation signal to distant oocytes. Development 132, 3357–3369.

Lee, M.H., Ohmachi, M., Arur, S., Nayak, S., Francis, R., Church, D., Lambie, E., Schedl, T., 2007. Multiple functions and dynamic activation of MPK-1 extracellular signal-regulated kinase signaling in *Caenorhabditis elegans* germline development. Genetics 177, 2039–2062.

Li, J., Ebata, A., Dong, Y., Rizki, G., Iwata, T., Lee, S.S., 2008. *Caenorhabditis elegans* HCF-1 functions in longevity maintenance as a DAF-16 regulator. PLoS Biol. 6, e233.

Liang, C.G., Su, Y.Q., Fan, H.Y., Schatten, H., Sun, Q.Y., 2007. Mechanisms regulating oocyte meiotic resumption: roles of mitogen-activated protein kinase. Mol. Endocrinol. 21, 2037–2055.

McCarter, J., Bartlett, B., Dang, T., Schedl, T., 1999. On the control of oocyte meiotic maturation and ovulation in *Caenorhabditis elegans*. Dev. Biol. 205, 111–128.

Mendenhall, A.R., LeBlanc, M.G., Mohan, D.P., Padilla, P.A., 2009. Reduction in ovulation or male sex phenotype increases long-term anoxia survival in a daf-16-independent manner in *Caenorhabditis elegans*. Physiol. Genomics 36, 167–178.

Miller, D.M., Shen, M.M., Shamu, C.E., Burglin, T.R., Ruvkun, G., Dubois, M.L., Ghee, M., Wilson, L., 1992. *C. elegans* unc-4 gene encodes a homeodomain protein that determines the pattern of synaptic input to specific motor neurons. Nature 355, 841–845.

Miller, M.A., Nguyen, V.Q., Lee, M.H., Kosinski, M., Schedl, T., Caprioli, R.M., Greenstein, D., 2001. A sperm cytoskeletal protein that signals oocyte meiotic maturation and ovulation. Science 291, 2144–2147.

Miller, M.A., Ruest, P.J., Kosinski, M., Hanks, S.K., Greenstein, D., 2003. An Eph receptor sperm-sensing control mechanism for oocyte meiotic maturation in *Caenorhabditis elegans*. Genes Dev. 17, 187–200.

Miller, M.A., Cutter, A.D., Yamamoto, I., Ward, S., Greenstein, D., 2004. Clustered organization of reproductive genes in the *C. elegans* genome. Curr. Biol. 14, 1284–1290.

Mor, A., Philips, M.R., 2006. Compartmentalized Ras/MAPK signaling. Annu. Rev. Immunol. 24, 771–800.

Nadarajan, S., Govindan, J.A., McGovern, M., Hubbard, E.J., Greenstein, D., 2009. MSP and GLP-1/Notch signaling coordinately regulate actomyosin-dependent cytoplasmic streaming and oocyte growth in *C. elegans*. Development 136, 2223–2234.

Neel, B.G., Gu, H., Pao, L., 2003. The 'Shp'ing news: SH2 domain-containing tyrosine phosphatases in cell signaling. Trends Biochem. Sci. 28, 284–293.

Nishimura, A.L., Mitne-Neto, M., Silva, H.C., Richieri-Costa, A., Middleton, S., Cascio, D., Kok, F., Oliveira, J.R., Gillingwater, T., Webb, J., Skehel, P., Zatz, M., 2004. A mutation in the vesicle-trafficking protein VAPB causes late-onset spinal muscular atrophy and amyotrophic lateral sclerosis. Am. J. Hum. Genet. 75, 822–831.

Ohmachi, M., Rocheleau, C.E., Church, D., Lambie, E., Schedl, T., Sundaram, M.V., 2002. *C. elegans* ksr-1 and ksr-2 have both unique and redundant functions and are required for MPK-1 ERK phosphorylation. Curr. Biol. 12, 427–433.

Page, B.D., Guedes, S., Waring, D., Priess, J.R., 2001. The *C. elegans* E2F- and DP-related proteins are required for embryonic asymmetry and negatively regulate Ras/MAPK signaling. Mol. Cell 7, 451–460.

Pendergrass, W., Wolf, N., Poot, M., 2004. Efficacy of MitoTracker Green and CMXrosamine to measure changes in mitochondrial membrane potentials in living cells and tissues. Cytom. A 61, 162–169.

Perkins, L.A., Larsen, I., Perrimon, N., 1992. corkscrew encodes a putative protein tyrosine phosphatase that functions to transduce the terminal signal from the receptor tyrosine kinase torso. Cell 70, 225–236.

Perkins, L.A., Johnson, M.R., Melnick, M.B., Perrimon, N., 1996. The nonreceptor protein tyrosine phosphatase corkscrew functions in multiple receptor tyrosine kinase pathways in *Drosophila*. Dev. Biol. 180, 63–81.

Posada, J., Cooper, J.A., 1992. Requirements for phosphorylation of MAP kinase during meiosis in *Xenopus* oocytes. Science 255, 212–215.

Praitis, V., Casey, E., Collar, D., Austin, J., 2001. Creation of low-copy integrated transgenic lines in *Caenorhabditis elegans*. Genetics 157, 1217–1226.

Ratnaparkhi, A., Lawless, G.M., Schweizer, F.E., Golshani, P., Jackson, G.R., 2008. A *Drosophila* model of ALS: human ALS-associated mutation in VAP33A suggests a dominant negative mechanism. PLoS ONE 3, e2334.

Reiner, D.J., Newton, E.M., Tian, H., Thomas, J.H., 1999. Diverse behavioral defects caused by mutations in *Caenorhabditis elegans* unc-43 CaM kinase II. Nature 402, 199–203.

Reinke, V., Smith, H.E., Nance, J., Wang, J., Van Doren, C., Begley, R., Jones, S.J., Davis, E.B., Scherer, S., Ward, S., Kim, S.K., 2000. A global profile of germline gene expression in *C. elegans*. Mol. Cell 6, 605–616.

Reinke, V., Gil, I.S., Ward, S., Kazmer, K., 2004. Genome-wide germline-enriched and sex-biased expression profiles in *Caenorhabditis elegans*. Development 131, 311–323.

Rosen, D.R., Siddique, T., Patterson, D., Figlewicz, D.A., Sapp, P., Hentati, A., Donaldson, D., Goto, J., O'Regan, J.P., Deng, H.X., et al., 1993. Mutations in Cu/Zn superoxide dismutase gene are associated with familial amyotrophic lateral sclerosis. Nature 362, 59–62.

Rothstein, J.D., 2009. Current hypotheses for the underlying biology of amyotrophic lateral sclerosis. Ann. Neurol. 65 (Suppl 1), S3–S9.

Schedl, T., Kimble, J., 1988. fog-2, a germ-line-specific sex determination gene required for hermaphrodite spermatogenesis in *Caenorhabditis elegans*. Genetics 119, 43–61.

Secondo, A., De Mizio, M., Zirpoli, L., Santillo, M., Mondola, P., 2008. The Cu-Zn superoxide dismutase (SOD1) inhibits ERK phosphorylation by muscarinic receptor modulation in rat pituitary GH3 cells. Biochem. Biophys. Res. Commun. 376, 143–147.

Seger, R., Krebs, E.G., 1995. The MAPK signaling cascade. FASEB J. 9, 726–735.

Sherwood, D.R., Butler, J.A., Kramer, J.M., Sternberg, P.W., 2005. FOS-1 promotes basement-membrane removal during anchor-cell invasion in *C. elegans*. Cell 121, 951–962.

Stetak, A., Gutierrez, P., Hajnal, A., 2008. Tissue-specific functions of the *Caenorhabditis elegans* p120 Ras GTPase activating protein GAP-3. Dev. Biol. 323, 166–176.

Tenenhaus, C., Schubert, C., Seydoux, G., 1998. Genetic requirements for PIE-1 localization and inhibition of gene expression in the embryonic germ lineage of *Caenorhabditis elegans*. Dev. Biol. 200, 212–224.

Tenenhaus, C., Subramaniam, K., Dunn, M.A., Seydoux, G., 2001. PIE-1 is a bifunctional protein that regulates maternal and zygotic gene expression in the embryonic germ line of *Caenorhabditis elegans*. Genes Dev. 15, 1031–1040.

Teuling, E., Ahmed, S., Haasdijk, E., Demmers, J., Steinmetz, M.O., Akhmanova, A., Jaarsma, D., Hoogenraad, C.C., 2007. Motor neuron disease-associated mutant vesicle-associated membrane protein-associated protein (VAP) B recruits wild-type VAPs into endoplasmic reticulum-derived tubular aggregates. J. Neurosci. 27, 9801–9815.

Timmons, L., Fire, A., 1998. Specific interference by ingested dsRNA. Nature 395, 854.

Timmons, L., Court, D.L., Fire, A., 2001. Ingestion of bacterially expressed dsRNAs can produce specific and potent genetic interference in *Caenorhabditis elegans*. Gene 263, 103–112.

Tsuda, H., Han, S.M., Yang, Y., Tong, C., Lin, Y.Q., Mohan, K., Haueter, C., Zoghbi, A., Harati, Y., Kwan, J., Miller, M.A., Bellen, H.J., 2008. The amyotrophic lateral sclerosis 8 protein VAPB is cleaved, secreted, and acts as a ligand for Eph receptors. Cell 133, 963–977.

Vazquez-Manrique, R.P., Gonzalez-Cabo, P., Ortiz-Martin, I., Ros, S., Baylis, H.A., Palau, F., 2007. The frataxin-encoding operon of *Caenorhabditis elegans* shows complex structure and regulation. Genomics 89, 392–401.

Whitten, S.J., Miller, M.A., 2007. The role of gap junctions in *Caenorhabditis elegans* oocyte maturation and fertilization. Dev. Biol. 301, 432–446.

Yanase, S., Onodera, A., Tedesco, P., Johnson, T.E., Ishii, N., 2009. SOD-1 deletions in *Caenorhabditis elegans* alter the localization of intracellular reactive oxygen species and show molecular compensation. J. Gerontol. A Biol. Sci. Med. Sci. 64, 530–539.